

## SODIUM -COBALT FERRITE NANOSTRUCTURE STUDY: SOL-GEL SYNTHESIS, CHARACTERIZATION, AND MAGNETIC PROPERTIES

A. M. EL NAHRAWY<sup>a,\*</sup>, A. A. SOLIMAN<sup>b</sup>, E. M. M. SAKR<sup>b</sup>,  
H. A. EL ATTAR<sup>b</sup>

<sup>a</sup>*Solid State Physics Department, Physics Research Division, National Research Centre (NRC)-33ElBohouthst, P.O.12622, Dokki, Giza, Egypt (Affiliation ID:60014618)*

<sup>b</sup>*Department of solid State Physics, Faculty of Women for Arts, Science and Education, Ain Shams University, Egypt*

The citrate sol gel reactions occurring in sodium co-doped cobalt ferrite nanoparticles (CFO NPs) with the chemical composition  $\text{Na}_x\text{Co}_{(1-x)}\text{Fe}_2\text{O}_4$  (where  $x = 0.25, 0.5, 0.75$ ) were synthesized and calcinated at  $800^\circ\text{C}$  for 3h. The crystalline phase and morphological analyses were investigated by using X-ray diffraction (XRD), high resolution scanning and transmission electron microscopy (HRSEM/HRTEM), Fourier transform infrared spectrometer (FT-IR) and vibrating sample magnetometer (VSM). The X-ray diffraction (XRD) pattern confirms a single phase cubic structure of pure and doped (CFO NPs). HRSEM and HRTEM results reveal that the prepared nanomagnetic are wall porous structures and spherical particles. The coercivity ( $H_{ci}$ ) varies from 1272.0 Oe to 625.93 Oe and the saturation magnetization ( $M_s$ ) ranges between 81.84 emu/g to 33.06 emu/g. The obtained results indicate that the citrate sol gel process is effective, low-cost and environment-friendly and play an important role in the synthesis, morphology, crystalline structure and magnetic property of spinel Na-Co $\text{Fe}_2\text{O}_4$  nanostructure.

(Received February 15, 2018; Accepted May 21, 2018)

*Keywords:* Spinel cobalt ferrite, Sol gel process, Magnetic nanostructures, Magnetic properties

### 1. Introduction

Spinel ferrites have a great attention regarding to their effective particle size dependent electronic, magnetic, chemical, mechanical and thermal properties [1–2]. Ferrites structures have practical applications in information storage systems, magnetic-electric, ferro-fluid technology, magnetocaloric refrigeration and magnetic diagnostics [3-5]. These magnetic materials are intensively influenced by their starting chemical composition and their microstructure, which are more sensitive to the manufacturing process [3]. Spinel ferrites have the general formula  $\text{AFe}_2\text{O}_4$  (where  $\text{A}^{2+} = \text{Co}, \text{Ni}, \text{Zn}, \text{Mg}, \text{etc.}$ ) and the unit cell contains 32 oxygen atoms in cubic cross-link packing with 8 tetrahedral ( $\text{T}_d$ ) and 16 octahedral ( $\text{O}_h$ ) occupied sites. Altering the divalent cation type and level content in the ferrites, enable us to obtain a large range of different physical and magnetic properties [6]. The basic uses of these spinel ferrites depend on the intrinsic properties such as Curie temperature, saturation magnetization, coercivity, phase, porosity, particle size, etc. Spinel ferrites have electro-magnetic properties owing to their ability to distribute the cations among the existing crystallographic lattice sites such as tetrahedral (A) and octahedral (B) sites [7, 8]. Cobalt ferrite nanostructure was suitable for a various applications in magnetic storage devices, electro-magnetic devices, electronic devices and in biomedical contrast imaging applications and devices [8-10]. Cobalt Ferrite ( $\text{CoFe}_2\text{O}_4$ ) as one the most practical spinel ferrites is an inverse spinel structured, hard ferrite magnetic material with moderate magnetization, high coercivity and narrow band gap ( $\sim 1.8$  eV) semiconducting oxide material [10, 11]. So, the introduction of different dopants in cobalt ferrite is an interesting strategy to modify its physicochemical properties. Synthesis technique, grain size, grain structure, porosity and cation distribution

---

\* Corresponding author: amany\_physics\_1980@yahoo.com

between the crystallites lattice sites are all factors that effectively impact the electrical and magnetic properties of (CFO) nanostructures [12]. The new characteristics of the magnetic materials such as high magneto resistance, quantum tunneling of the magnetization, and super paramagnetism are attributed to the small size and high surface area of magnetic particles [12, 13]. Since, the synthetic method is greatly affect the physicochemical properties of nano-ferrites, different methods were applied for the synthesis of (CFO) NPs such as hydrothermal synthesis [14], sol–gel method [15, 16], ball milling [17], and chemical precipitation [18].

Sol–gel technology introduces a versatile chemical manner for the synthesis of inorganic nanoparticles and organic–inorganic nano-composites [19, 20]. Since sol–gel processes can occur under extraordinarily low thermal treatment conditions, and due to the fascinating and unique combinations of properties and interesting advantages such as high homogeneity and purity, controllability of size and shape, and enhanced high surface area, sol–gel technology has established increasing applications in a various range of scientific research and industrial fields [21].

Hence, in this work we have investigated the sol gel synthesis, structural and magnetic characterizations of sodium doped cobalt ferrite nanostructures with the chemical composition  $\text{Na}_x\text{Co}_{1-x}\text{Fe}_2\text{O}_4$  (where  $x = 0.00, 0.25, 0.5$  and  $0.75$ ), calcined at  $800^\circ\text{C}$  for 3hs. The nanostructures produced were characterized by the following techniques: X-ray diffraction (XRD), high resolution transmission and scanning electron microscopy (RHTM/HRSEM), Fourier transform infrared (FT-IR) and vibrating sample magnetometer (VSM).

## 2. Experimental work

### 2.1 Raw materials and preparation

Sodium co-doped cobalt ferrite nanoparticles (Na-CFO) having the formula  $\text{Na}_x\text{Co}_{1-x}\text{Fe}_2\text{O}_4$  (where  $x = 0.00, 0.25, 0.5, 0.75$ ) were synthesized by citrate-gel method. The used precursors were cobalt nitrate ( $\text{Co}(\text{NO}_3)_2 \cdot 6\text{H}_2\text{O}$ ), iron (III) nitrate ( $\text{Fe}(\text{NO}_3)_3 \cdot 9\text{H}_2\text{O}$ ), sodium nitrate ( $\text{NaNO}_3$ ) and citric acid ( $\text{C}_6\text{H}_8\text{O}_7 \cdot \text{H}_2\text{O}$ ). A stoichiometric amount of all metal nitrates were dissolved in distilled water/ citric acid and mixed together under vigorous magnetic stirring, to obtain a homogeneous solution. The addition of citric acid as a catalyst helps in the segregation and homogeneous distribution of the magnetic metal ions [22]. Then, the resultant solutions were slowly evaporated at  $200^\circ\text{C}$  until a gel - xerogel formed in air, to remove solvent molecules from the mixture. During this process, the initial deep brown color of the solution changed to a highly viscous gel. Finally, calcination at  $800^\circ\text{C}$  for 3h, of xerogel for pure and doped leads to the formation of dense nanopowder of Na-CFO.

### 2.2 Characterization of Na-CFO nanoparticles

The structural characterization of synthesized Na-CFO nanoparticles was carried out by X-ray Bruker-D8 advance diffractometer (XRD) using monochromatized  $\text{CuK}\alpha$  radiation of wavelength ( $\lambda$ ) =  $1.54056 \text{ \AA}$  operated at 40 kV and 40 mA. Scans were performed with a detector step size of  $0.02^\circ$  over an angular range of  $2\theta$  starting from  $10$  to  $80^\circ$ . The magnetic nanoparticles average sizes were calculated using Scherrer's equation [23]:

$$D = \frac{0.9\lambda}{\beta \cos\theta} \quad (1)$$

where  $D$  is the average grain size along the direction vertical to the certain crystal plane referring to grain size,  $\lambda$  is the X-ray wavelength ( $= 1.54056 \text{ \AA}$ ),  $\beta$  is the peak width in radians, measured at half of the maximum intensity, and  $\theta$  is the Bragg diffraction angle,  $d$ -spacing is calculated by using Bragg's Law. The surface morphology of the as-prepared samples was investigated using high resolution scanning electron microscope (HRSEM), (JEM-1230). Samples were coated with gold at 10 mA for 2 min prior to SEM analysis. High resolution transmission electron microscope (HRTEM), JEOL, JEM-2100. Fourier transform infrared (FTIR) spectra of the as-prepared

samples were recorded with a FT-IR spectrometer (Nicolet Impact-400 FT-IR spectrophotometer) in the range of 200– 4000  $\text{cm}^{-1}$ . The dried samples were ground into very fine powder and then blended with KBr before pressing the mixture into ultra-thin pellets. The room temperature magnetic hysteresis loops of the prepared nanomagnetic samples were measured by vibrating sample magnetometer (VSM) Model: Lake shore 7410.

### 3. Results and discussion

#### 3.1 X-ray Diffraction (XRD)

Fig. 1 shows the XRD patterns of pure  $\text{CoFe}_2\text{O}_4$  (CFO) and  $\text{Na}_x\text{Co}_{(1-x)}\text{Fe}_2\text{O}_4$  (where  $x=0.25, 0.5$  and  $0.75$ ) nanoparticles prepared using sol gel process and calcined at  $800^\circ\text{C}$  for 3h. The resulted XRD patterns revealed the high crystallinity degree of the formed nanoparticles samples and confirmed the spinel CFO phase according to (JCPDS, Card no. 22-1086), indicating that single phase spinel cubic structure with space group  $\text{Fd}\bar{3}\text{m}$  are successfully formed for pure and doped (CFO). Also, no impurity phase has been identified with incorporation Na ions in CFO any of the samples. The XRD peaks can be indexed to (111), (220), (311), (400), (422), (511) and (440) crystal planes as the fundamental of the cubic  $\text{CoFe}_2\text{O}_4$  nanoparticles. In addition, the intense of the (311) peak increases indicating the higher crystallinity degree while the intensity of the (111), (222) and (422) peaks weakens with the incorporation of Na ions. The average crystallite size of the prepared samples (D) was calculated for the most intense peaks of each sample by Sherrer's formula [23]. The estimated crystallite size was found to be about 29 nm, 27.5 nm, 26 nm and 28 nm for (CFO), ( $\text{Na}_{0.25}\text{Co}_{0.75}\text{Fe}_2\text{O}_4$ ), ( $\text{Na}_{0.5}\text{Co}_{0.5}\text{Fe}_2\text{O}_4$ ) and ( $\text{Na}_{0.75}\text{Co}_{0.25}\text{Fe}_2\text{O}_4$ ), respectively. Where, the upper limit of crystallite size is very significant for successful spinning [24]. There is a small shift in the position of the peak (311) and relative decrease in the intensity of all the peaks, corresponding to the incorporation of  $\text{Na}^{1+}$  ions in pure (CFO) network, this is may be imputed to the decrease of the total molecular weight of the prepared nanomagnetic samples by the introduction of the lighter  $\text{Na}^{1+}$  ions than  $\text{Co}^{3+}$  ions in (CFO) nanoparticles [25]. The values of average crystallite sizes (D), lattice parameter (a) (experimental and theoretical) the surface area and strain of the prepared magnetic samples are shown in table (1). From the table it is appeared that, the increase in the lattice constant (a) is due to the difference in ionic radii of  $\text{Na}^{1+}$  ( $1.02 \text{ \AA}$ ) as compared to  $\text{Co}^{3+}$  ( $0.72 \text{ \AA}$ ) [25, 26]. Therefore when the larger  $\text{Na}^{1+}$  ions were replaced with the smaller  $\text{Co}^{3+}$  ions in octahedral sites and cause the increase in the lattice parameter (a), causes strain of unit cell dimensions, that way increasing the lattice parameter [26]. Estimated values of average crystallite sizes (D in nm) lattice parameters (a in  $\text{A}^\circ$ ) and strain are tabulated in Table 1.

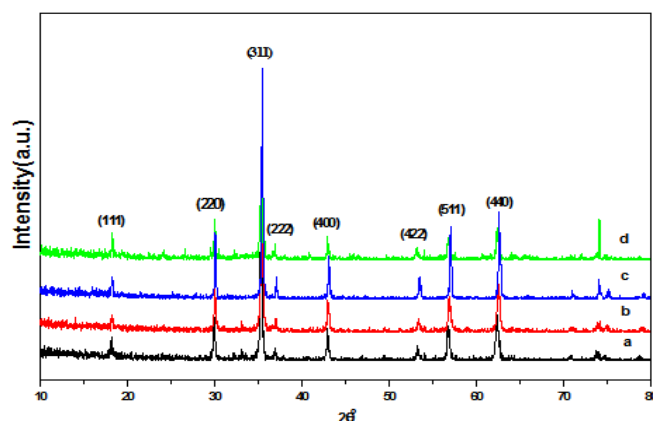


Fig.1. The XRD patterns for  $\text{Na}_x\text{Co}_{(1-x)}\text{Fe}_2\text{O}_4$  with  $x = 0.0, 0.25, 0.5$  and  $0.75$ , calcined at  $800^\circ\text{C}$ .

Table 1. Shows the values of crystallite size ( $D$ ) and lattice parameter ( $a$ ) with the substitution of  $\text{Na}^{1+}$  ions into CFO.

Sample	Crystallite size ( $D$ ) (nm)	d-spacing ( $\text{Å}^\circ$ )	Exp.Lattice parameter ( $a$ ) ( $\text{Å}^\circ$ )	theoretical lattice parameter	Molecular weight (M)(a.m.u)	X-ray Density ( $D_x$ ) $\text{g/cm}^3$	Specific surface area ( $\text{m}^2/\text{g}$ )	Strain ( $\epsilon$ )
$\text{CoFe}_2\text{O}_4$	29	2.53210	8.39803	8.39470	234.621	5.262	39.319	0.201
$\text{Na}_{0.25}\text{Co}_{0.75}\text{Fe}_2\text{O}_4$	28	2.53509	8.40794	8.39773	225.635	5.043	41.026	0.215
$\text{Na}_{0.5}\text{Co}_{0.5}\text{Fe}_2\text{O}_4$	26.3	2.54240	8.44219	8.42195	216.649	4.800	47.529	0.270
$\text{Na}_{0.75}\text{Co}_{0.25}\text{Fe}_2\text{O}_4$	28.3	2.53966	8.42310	8.41286	207.663	4.616	45.930	0.216

### 3.2 Scanning and transmission electron microscopy (HRSEM-HRTEM):

Fig. 2 shows the HRSEM (a-c) and HRTEM (d, e) images of the prepared  $\text{Na}_x\text{Co}_{(1-x)}\text{Fe}_2\text{O}_4$  (where  $x = 0.0, 0.5$  and  $0.75$ ) nanoparticles calcined at  $800^\circ\text{C}$ , which appear the common morphology of composite ceramics. As could be observed in Fig. 2(a,b), the surface morphology of CFO doped with (0.0, 0.5) content of  $\text{Na}^{1+}$  ions, the samples exhibited a mix of curved flake-shaped condensed structure with some nanospheres on the flake surfaces and nanorods linking between them and distributed on their surfaces of nano-scale, which is similar to that reported in Ref.[27]. The HR-SEM image of the sample  $\text{Na}_{0.75}\text{Co}_{0.25}\text{Fe}_2\text{O}_4$  is shown in the Fig.2 (c). As seen, the flake-shaped structure and the clusters of smaller particles were altered to a spongy-shaped structure with a high porosity as we expected from the XRD examination which enhance the properties of such a magnetic material. The surface morphology of the prepared CFO doped with Na ions were due to aggregation of nano-magnetic and gathering in flakes or sheets and nano-rod like morphology. Indeed, the flakes or sheet and nano-rod-like morphology was confirmed by HR-TEM observations, as in Fig. 2(d, e). Fig. 2 (d, e) presents the results of CFO doped with (0.5, 0.75) content of  $\text{Na}^{1+}$  ions. The images reveal that the prepared nanoparticles were spherical shape and with relative agglomeration. The clear agglomeration is attributed to the existence of dipolar field in crystallites (magnetic nature) of Na-CFO (NPs). It is obvious the uniform particle size distribution and almost all nanoparticles were with average particle size 25 nm. The produced values are in good agreement with the crystallite size obtained from the XRD patterns.

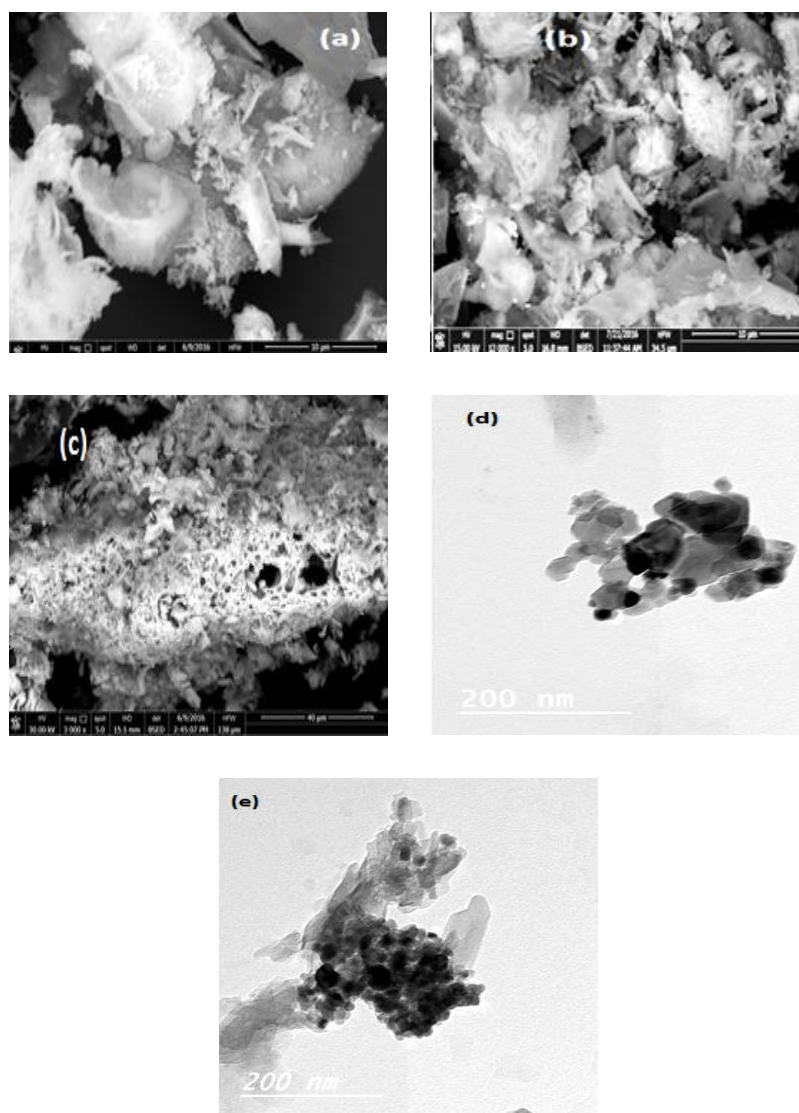


Fig. 2 (a–c): HRSEM and (d, e) HRTEM images for  $\text{Na}_x\text{Co}_{(1-x)}\text{Fe}_2\text{O}_4$  for (a)  $x=0.0$ , (b, d)  $x=0.5$  and (c, e)  $x=0.75$ , calcined at  $800^\circ\text{C}$  for 3h.

### 3.3 Fourier Transform Infrared Spectroscopy (FTIR) analysis

Fourier transform infrared (FT-IR) analysis was applied to investigate the presence of functional groups (the metal-oxygen bonding) and impurity on the surface of the prepared samples, where the IR absorption bands of solids matrices are usually ascribed to the vibration of ions in the crystal lattice [28]. FTIR spectra of the prepared nanomagnetic samples are shown in Fig. 3. It is clear from Fig. 3, there is a broad band at around  $3447\text{ cm}^{-1}$  referring the structural O-H and the band at  $1615\text{ cm}^{-1}$  attributed to the deformation mode of OH groups in the internal structure of pure and doped CFO nanoparticles [28, 29]. There is some weak absorption peaks at  $2918$ ,  $2847$ ,  $1727$  and  $1433\text{ cm}^{-1}$  in the FTIR spectra were ascribed to the stretching vibration mode of C–H bond from the residual solvents [30]. The CFO-based nanoparticles have the absorption band at  $1196\text{ cm}^{-1}$  that shifted to the lower wavelength values with incorporation Na ions at, may be due to the vibrations of the bond between Oxygen ion and octahedral metal ion  $\text{M}_{\text{octa}}\leftrightarrow\text{O}$  [31]. The absorption bands located at  $400\text{--}700\text{ cm}^{-1}$  are attributed to the vibrations of the ions of the crystal lattice in spinel ferrites. The two significant absorption bands, at around  $575\text{ cm}^{-1}$  and  $467\text{ cm}^{-1}$  for pure (CFO) and shifted to the lower wavelength ( $565\text{ cm}^{-1}$ ) with incorporation of Na ions in (CFO) matrix, that are the common features of spinel ferrites [32, 33]. The absorption band at  $500\text{--}600\text{ cm}^{-1}$  was attributed to stretching vibrations of  $\text{Fe}^{3+}\text{-O}^{2-}$  tetrahedral site, which were

appeared in most of the ferrites matrices [34]. The main strong absorption bands in the range 400-700  $\text{cm}^{-1}$  reveal the formation of single phase spinel structure are assigned to the stretching vibrations mode of the spinel unit cell in the tetrahedral (A) site and the metal–oxygen vibrations in the octahedral (B) site [35]. Also, the obtained result is in agreement with that of Waldron and Kurtan, ascribed the high frequency bands to the tetrahedral group (around 600-700  $\text{cm}^{-1}$ ) and low frequency band to the octahedral group (around 350-450  $\text{cm}^{-1}$ ) [35, 36].

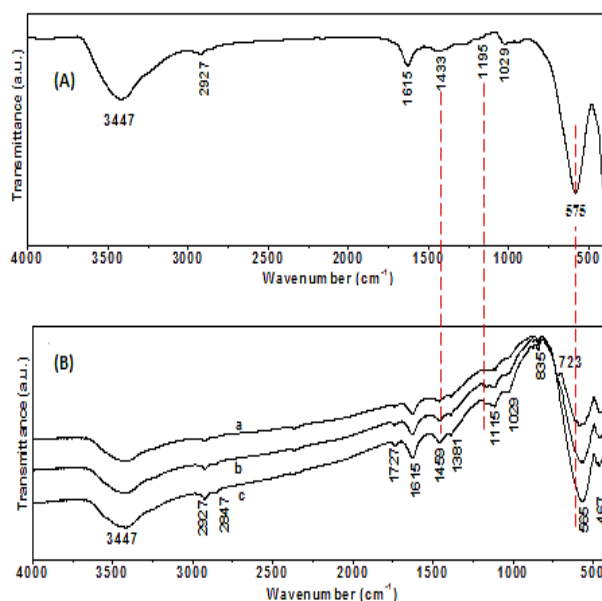


Fig. 3. FT-IR spectra of (A) CFO and (B)  $\text{Na}_x\text{Co}_{(1-x)}\text{Fe}_2\text{O}_4$  nanoparticles for (a) 0.25, (b) 0.5, and (c) 0.75, calcined at 800°C.

### 3.4 Magnetic measurements

The typical hysteresis loops of  $\text{Na}_x\text{Co}_{(1-x)}\text{Fe}_2\text{O}_4$  ( $x = 0.25, 0.5, 0.75$ ) calcined at 800°C for 3h, were shown in Fig. 4. Fig. 4 indicates the dependences of magnetization (M) values on the applied field (H), M -H loops of the prepared samples  $\text{CoFe}_2\text{O}_4$  and Na doped  $\text{CoFe}_2\text{O}_4$  measured at room temperature, which are distinguishing of ferromagnetic behavior. The saturation magnetization value ( $M_s$ ) is 81.846 emu/g for the as-prepared pure  $\text{CoFe}_2\text{O}_4$ , as tabulated in table 2. The values of saturation magnetization ( $M_s$ ) decreased from 81.84 emu/g to 33.06 emu/g with increasing the  $\text{Na}_2\text{O}$  concentration in CFO matrix due to the gradual rearrangement in the internal structure (i.e., crystallinity and particle scale) and might be the occupancy of lesser magnetic  $\text{Na}^{1+}$  ions in the tetrahedral A-sites [37]. The introducing of nonmagnetic Na ions in magnetic Co ions lowers the magnetization values. The values of the coercivity ( $H_{ci}$ ) rapidly changed from 1272.0 Oe, 707.27 Oe, 163.4 Oe and 625.93 Oe with incorporation of  $\text{Na}_2\text{O}$  dopant at  $x = 0.0, 0.25, 0.5$  and 0.75, which is due to the replacement of  $\text{Co}^{3+}$  ions causing grain growth in Na-CFO nanoparticles decreasing the coercivity as a whole. All doped samples display the small ( $H_{ci}$ ) values because pure  $\text{CoFe}_2\text{O}_4$  is considered a typical soft magnetic material. The remanent magnetization ( $M_r$ ) values in the range from 36.875 to 9.6679 emu/g. The hysteresis loop results for Na-CFO show that the introduction of nonmagnetic Na ions really plays key role for changing the ( $M_s$ ) values of the samples.

Table 2. Magnetic properties, Saturation magnetization ( $M_s$ ), Coercivity ( $H_c$ ) and Remnant magnetization ( $M_r$ ) of obtained Na-CFO nanoparticles.

Sample	$M_s$ (emu)	$M_r$ (emu/g)	$H_{ci}$ (G)	Squareness ( $M_r/M_s$ )
$\text{CoFe}_2\text{O}_4$	81.846	36.875	1272	0.35989
$\text{Na}_{0.25}\text{Co}_{0.75}\text{Fe}_2\text{O}_4$	65.951	6.6951	163.40	0.10151
$\text{Na}_{0.5}\text{Co}_{0.5}\text{Fe}_2\text{O}_4$	61.404	20.155	706.45	0.32824
$\text{Na}_{0.75}\text{Co}_{0.25}\text{Fe}_2\text{O}_4$	33.061	9.6679	627.24	0.29243

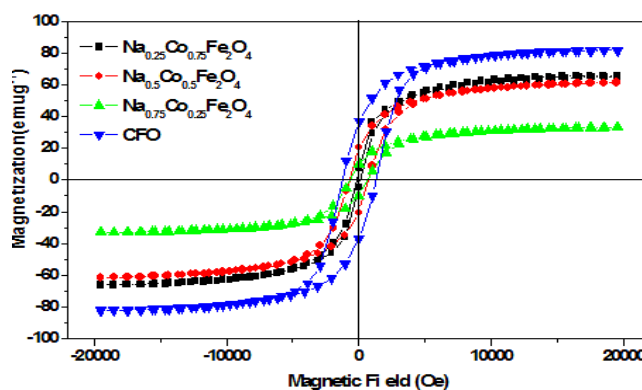


Fig. 4. Magnetic hysteresis loops of the samples CFO and  $\text{Na}_x\text{Co}_{(1-x)}\text{Fe}_2\text{O}_4$  nanoparticles ( $x = 0.25, 0.5, \text{ and } 0.75$ ), calcined at  $800^\circ\text{C}$ .

#### 4. Conclusions

The aim of this work is to construct magnetic nanoparticles based on  $\text{CoFe}_2\text{O}_4$  and doped with Na ions with modified magnetization, morphology and good chemical stability were successfully prepared using citrate sol gel process and calcined at  $800^\circ\text{C}$  for 3h in air.

The  $\text{CoFe}_2\text{O}_4$  nanoparticles were select as the studying base because it has the highest magnetization. X-ray diffraction (XRD) analyses confirm the formation of the cubic phase spinel structure without any impurity phase and the calculated crystallite sizes of the prepared Na-CFO are in the range of 29-28 nm.

The nanomagnetic samples show hysteresis loop which indicates the soft and hard phases are well exchange coupled under the effect of Na ions. The Na-CFO coercivity varies from 1272.0 Oe to 625.93 Oe and the saturation magnetization ranges from 81.84 emu/g to 33.06 emu/g with increasing the  $\text{Na}_2\text{O}$  concentration in CFO matrix.

#### References

- [1] Y. Z. Donga, S. H. Piao, K. Zhang, H. J. Choi, Colloids and Surfaces A **537**, 102 (2018).
- [2] J. Dong, Y. Zhang, X. Zhang, Q. Liu, J. Wang, Materials Letters **120**, 9 (2014).
- [3] M. R. Bhandare, H. V. Jamadar, A.T. Pathan, B. K. Chougule, A. M. Shaikh, J. Alloys Compd. **509**, L113 (2011).
- [4] P. P Hankare, R. P.Patil, K. M Garadkar, Mater. Res. Bull. **46**, 447 (2011).
- [5] N. Dong, F. He, J. Xin, Q. Wang, Z. Lei, B. Su, Materials Letters **141**, 238 (2015).
- [6] M. Sertkol, Y. Köseoglu, A. Baykal, H. Kavas, A. M. S. Bozkurt, M. S. Toprak, J. Alloys Compd. **486**, 325 (2009).
- [7] V. A. M.Brabers, Handbook of Magnetic Materials **8**, North-Holand, Amsterdam, 189, 1995.

- [8] R. Topkaya, U. Kurtan, Y. Junejo, A. Baykal, *Materials Research Bulletin* **48**, 3247 (2013).
- [9] S. Abdul Khader, T. Sankarappa, T. Sujatha, J. S. Ashwajeet, R. Ramanna, *Materials Today: Proceedings* **2**, 4334 (2015).
- [10] S. Singh, S. Munjal, N. Khare, J. Magn. Magn. Mater. **386**, 69 (2015).
- [11] M. Cvek, M. Mrlik, V. Pavlinek, *J. Rheol.* **60**, 687 (2016).
- [12] D. Jamon, E. Marin, S. Neveu, M.-F. Blanc-Mignon, F. Royer, *Photonics and Nanostructures – Fundamentals and Applications* **27**, 49 (2017).
- [13] Na. S. Kumar, N. S. Kumar, K. V. Kumar, *World Journal of Nano Science and Engineering* **5**, 140 (2015).
- [14] S. C. Goh, C. H. Chia, S. Zakaria, M. Yusoff, C. Y. Haw, S. H. Ahmadi, N. M. Huang, H. N. Lim, *Mater. Chem. Phys.* **120**, 31 (2010).
- [15] H. Cui, Y. Jia, W. Ren, W. Wang, *J. Sol–Gel Sci. Technol.* **55**, 36 (2010).
- [16] X. W. Wang, Y. Q. Zhang, H. Meng, Z. J. Wang, Z. D. Zhang, *Journal of Alloys and Compounds* **509**, 7803 (2011).
- [17] P. M. Richard, C. Yenny, P. Vargas, J. Silva, O. N. C. Uwakweh, *Mater. Char.* **61**, 1317 (2010).
- [18] J. Wang, D. Tong, Y. Lin, C. Yang, W. Zhan, *J. Alloys Comp.* **450**, 532 (2008).
- [19] Y. Koseoğlu, A. Baykal, S. M. Toprak, F. Gozuak, C. A. Bas Aran, B. Aktas, *J. Alloys Compd.* **462**, (2008)..
- [20] A. M. Elnahrawy, Y. S. Kim, A. I. Ali, *Journal of Alloys and Compounds* **676**, 432 (2016).
- [21] J. D. Mackenzie, D. R. Ulrich (Editors), *Ultrastructure Processing of Advanced Ceramics*, Wiley, New York, 1988.
- [22] P. Sivakumar, R. Ramesh, A. Ramanand, S. Ponnusamy, C. M. Hchelvan, *Applied Surface Science* **258**, 6648 (2012).
- [23] A. M. Amer, T. Meaz, M. Yehia, S. S. Attalah, F. Fakhry, *Alloys Compd.* **633**, 448 (2015).
- [24] O. M. Hemed, *Turk J. Phys.* **28**, 121 (2004).
- [25] M. Zukalová, B. P. Lásková, M. Klementová, L. Kavan, *Electrochimica Acta* **245**, 505 (2017).
- [26] R. L. Ciceo, M. Todea, R. Dudric, A. Buhai, V. Simon, *Journal of Non-Crystalline Solids* **481**, 562 (2018).
- [27] C. Fei, Y. Zhang, Z. Yang, Y. Liu, R. Xiong, J. Shi, X. Ruan, *Journal of Magnetism and Magnetic Materials* **323**, 1811 (2011).
- [28] S. Anjum, F. Sehar, F. Bashir, M. S. Awan, Z. Mustafa, *Materials Today: Proceedings* **2**, 5182 (2015).
- [29] B. Behshid, K. Ahmad, S. Hojjat, V. V. Sabino, R. C. Jesus, M. M. del Puerto, Mozaffari Morteza, 5th European IFMBE Conference, *IFMBE Proceedings* **37**, 1370 (2011).
- [30] A. Baykal, S. Esir, A. Demir, S. Güner, *Ceramics International* **41**, 231 (2015).
- [31] A. Baykal, N. Kasapoğlu, Y. Köseoğlu, S. Muhammet Toprak, H. Bayrakdar, *Journal of Alloys and Compounds* **464**, 514 (2008).
- [32] M. Hashim, Alimuddin, E. S. Shirsath, S. Kumar, R. Kumar, S. A. Roy, J. Shah, K. R. Kotnala, *J. Alloys and Compounds* **549**, 348 (2013).
- [33] Y. Mohammadifar, H. Shokrollahi, Z. Karimi, L. Karimi, *J. Magn. Magn. Mater.* **366**, 44 (2014).
- [34] V. Jadhav, P. Chikode, G. Nikam, S. Sabale, *Materials Today: Proceedings* **3**, 4121 (2016).
- [35] R. D. Waldron, *Physical Review* **99**, 1727 (1955)  
<http://dx.doi.org/10.1103/PhysRev.99.1727>.
- [36] U. Kurtan, R. Topkaya, A. Baykal, M. S. Toprak, *Ceramics International* **39**, 6551 (2013).
- [37] S. Bhukal, S. Mor, S. Bansal, J. Singh, S. Singhal, *Journal of Molecular Structure* **1071**, 95 (2014).